PHYSICAL REVIEW A **98**, 011401(R) (2018)

Rapid Communications

Tailored orbital angular momentum in high-order harmonic generation with bicircular Laguerre-Gaussian beams

Willi Paufler,[1,2,*] Birger Böning,[1] and Stephan Fritzsche[1,2]
[1]Theoretisch Physikalisches Institut, Friedrich Schiller Universität, 07743 Jena, Germany
[2]Helmholtz Institut, 07743 Jena, Germany

(Received 9 April 2018; published 6 July 2018)

We report on a method to generate extreme ultraviolet vortices from high-order harmonic generation with two-color counter-rotating Laguerre-Gaussian (LG) beams that carry a well-defined orbital angular momentum (OAM). Our calculations show that the OAM of each harmonic can be directly controlled by the OAM of the incident LG modes. Furthermore, we show how the incoming LG modes have to be tailored, in order to generate every possible value of OAM in the emitted harmonics. In addition, we analyze the emitted harmonics with respect to their divergence and find that it decreases with the harmonic order and increases with the OAM of the emitted harmonic.

DOI: 10.1103/PhysRevA.98.011401

Light beams are known to carry a spin angular momentum (SAM) of ± 1, which is associated with their polarization. Allen *et al.* [1] demonstrated that light beams can additionally carry a well-defined orbital angular momentum (OAM) of ℓ, which is related to the transverse spatial profile. Laguerre-Gaussian (LG) modes, which are solutions of the paraxial wave equation, are the most common light beams with such a property. Their spatial profile contains an azimuthal phase dependence $e^{i\ell\phi}$, which results in a helical phase front [2]. Therefore, such beams are often referred to as *twisted light* beams. The absorption of photons from such twisted beams by atoms or molecules offers rich light-matter interactions beyond the plane-wave selection rules [3,4]. For example, ionization of atoms by twisted light modifies the electron wave packet and gives rise to different dichroism signals besides the well-known circular dichroism [5]. Moreover, optical vortices have been applied as a tool to trap particles [6] or to detect spinning objects [7]. The wide range of applications of twisted light beams indeed stimulated extensive research on the generation of vortex beams up to the extreme ultraviolet (XUV) region.

High-order harmonic generation (HHG) has been found to be a versatile source to generate XUV vortex beams [8–11]. It can be understood in terms of a simple semiclassical three-step model [12], where a valence shell electron is (i) first released from the atom via tunnel ionization, (ii) subsequently driven by the oscillating laser field in the continuum, and (iii) may recombine with its parent ion under the emission of a highly energetic photon up to the XUV region.

During recent years, therefore, the synthesis and characterization of XUV beams with OAM due to HHG became a highly active field of research. It was demonstrated that the qth harmonic not only has q times the frequency ω but also q times the OAM ℓ of the fundamental beam, if the harmonics are created by a single linearly ($\omega \leftrightarrow$) polarized LG mode [9,10],

$$\mathrm{LG}_{\ell,0}^{\omega\leftrightarrow} \xrightarrow{\mathrm{HHG}} \begin{array}{rcl} \omega_{H_q} & = & q\,\omega, \\ \ell_{H_q} & = & q\,\ell. \end{array}$$

Here, ω and ω_{H_q} denote the frequencies and ℓ and ℓ_{H_q} the OAM of the incident LG mode and the qth harmonic, respectively. The even harmonics are suppressed due to the symmetry of the field [13,14]. In contrast to HHG with linearly polarized beams, where the emitted harmonics are linearly polarized, circularly polarized harmonics can be generated by two-color counter-rotating ($\omega \circlearrowright + 2\omega \circlearrowleft$), called bicircular, fields (cf. Fig. 1). Here, every third harmonic is suppressed and the other harmonics exhibit alternating helicities [cf. Fig. 1(d)] [15–17].

For bicircular fields, the HHG can be explained within an intuitive photon picture by conservation of energy and SAM [18–21] and summarized by the following selection rules,

$$\mathrm{LG}_{0,0}^{\omega\circlearrowright} \oplus \mathrm{LG}_{0,0}^{2\omega\circlearrowleft} \xrightarrow{\mathrm{HHG}} \begin{array}{rcl} \omega_{H_q} = q\,\omega & = & m\,\omega + n\,2\omega, \\ m-n & = & \pm 1, \\ \ell_{H_q} & = & 0, \end{array} \tag{1}$$

where m and n denote the number of photons with frequency ω and 2ω, respectively. $\mathrm{LG}_{0,0}$ is a Gaussian beam with zero OAM and as the incident beams, also the harmonics carry zero OAM.

In this Rapid Communication, we investigate HHG with two-color counter-rotating LG modes and show that the selection rules for bicircular fields have to be extended in order to include conservation of OAM:

$$\mathrm{LG}_{\ell_1,0}^{\omega\circlearrowright} \oplus \mathrm{LG}_{\ell_2,0}^{2\omega\circlearrowleft} \xrightarrow{\mathrm{HHG}} \begin{array}{rcl} \omega_{H_q} = q\omega & = & m\omega + n2\omega, \\ m-n & = & \pm 1, \\ \ell_{H_q} & = & m\,\ell_1 + n\,\ell_2, \end{array} \tag{2}$$

*willi.paufler@uni-jena.de

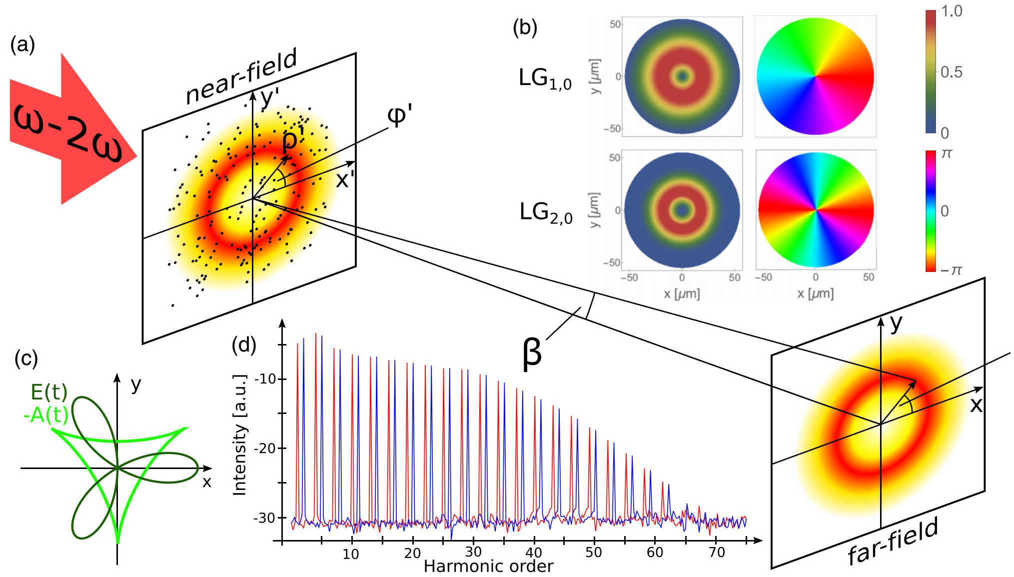

FIG. 1. Scheme of HHG with bicircular LG beams. The setup is shown in the center of (a). The incident beam is a superposition of a circularly polarized $LG^{\omega\circlearrowleft}$ mode with its counter-rotating second harmonic $LG^{2\omega\circlearrowright}$ of the same intensity. The gas target is approximated by a thin layer at the focus of the beam extended over the whole beam, which is indicated by the black dots in the near field. At each point in the gas target harmonics are emitted. The emitted harmonics contribute to the far field. The intensity and phase profile of a $LG_{1,0}$ and a $LG_{2,0}$ mode are displayed in (b), while (c) shows the electric field (dark green) and the vector potential (light green) of a ω-2ω bicircular field. Finally, a sketch of the emitted harmonics in a bicircular field is shown in (d). The harmonics exhibit the polarization of the incident beam with the fundamental frequency ω (red) followed by a harmonic with the polarization of the incident second harmonic (blue). Every third harmonic is suppressed for a ω-2ω bicircular field.

where ℓ_1 and ℓ_2 denote the OAM of the incident beams. The selection rules (2) allow a direct control of the OAM of the harmonics by the OAM of the incident beams. In our simulations we choose the propagation axis of the LG beams to coincide with the z axis. In cylindrical coordinates, the spatial structure of a LG mode can be expressed as

$$\begin{aligned}\mathrm{LG}_{\ell,p}(\rho,\phi,z) &= E_0\frac{W_0}{W(z)}\left(\frac{\rho}{W(z)}\right)^{|\ell|}L_p^{|\ell|}\left[\frac{2\rho^2}{W^2(z)}\right]\exp\left(-\frac{\rho^2}{W^2(z)}\right)\\ &\quad\times\exp\left(ik\frac{\rho^2}{2R(z)}+i\Phi_G(z)+i\ell\phi\right),\end{aligned} \tag{3}$$

where W_0 is the beam waist, $W(z)=W_0\sqrt{1+\frac{z}{z_0}}$ is the beam width, $z_0=k\frac{W_0^2}{2}$ is the Rayleigh range, $R(z)=z(1+\frac{z_0^2}{z^2})$ is the phase front radius, $\Phi_G(z)=-(|\ell|+2p+1)\arctan(\frac{z}{z_0})$ is the Gouy phase, and $L_p^{|\ell|}[x]$ are the associated Laguerre polynomials. As before, the index ℓ denotes the OAM of the beam and the index p is associated with the number of radial nodes of the beam. In our simulations we have chosen $p=0$ and $W_0=30\ \mu$m for the $LG_{1,0}$ beam. We make use of a superposition of two incident beams with combinations of OAM $(\ell_1,\ell_2)=(1,1),(1,2)$, and $(2,1)$, respectively. The waist W_0 of the $LG_{2,0}$ beam was adjusted, such that the the radii of the intensity maxima coincide for both the $LG_{1,0}$ and the $LG_{2,0}$ beam [cf. Fig. 1(b)] as in Ref. [22]. The intensity maximum of each beam is chosen as 10^{14} W/cm^2 at the focus. We here approximate our atomic gas target by a two-dimensional thin layer of equally distributed atoms across the focus of the beam, as indicated by the black dots in the near field in Fig. 1(a). At each point of the two-dimensional target, moreover, we calculate the time-dependent dipole moment for a hydrogen atom as derived by Lewenstein *et al.* [23]. For our calculations we used the RB-SFA code [24]. In order to calculate the frequency spectrum of the emitted harmonics in the near field, we perform a Fourier transform of the time-dependent dipole moment at each point of our two-dimensional gas target. The far-field phase and intensity profiles are calculated by using the Fraunhofer diffraction formula [25]. The complex amplitude of the qth harmonic in the far field can be written as

$$\begin{aligned}A_q^{\mathrm{far}}(\beta,\phi) &= \int_0^\infty\int_0^{2\pi}\rho' d\rho' d\phi' A_q^{\mathrm{near}}(\rho',\phi',z')\\ &\quad\times\exp\left(-i\frac{2\pi}{\lambda_q}\rho'\tan(\beta)\cos(\phi-\phi')\right),\end{aligned} \tag{4}$$

with the wavelength $\lambda_q=\lambda/q$ of the qth harmonic and where $A_q^{\mathrm{near}}(\rho',\phi',z')$ is the complex amplitude of the qth harmonic in the near field, ϕ is the polar angle in the far field, and β is the angle of divergence [cf. Fig. 1(a)].

Figure 2 displays the far-field phase (left) and intensity (right) profiles for the 13th and 14th harmonic for three different superpositions of two incident LG modes. While the fundamental beam $LG_{\ell_1,0}^{\omega\circlearrowleft}$ has frequency $\omega=0.057$ a.u. and carries a SAM of 1, the second beam $LG_{\ell_2,0}^{2\omega\circlearrowright}$ has frequency 2ω and carries a SAM of -1. In the upper row, both incident beams carry an OAM of $\ell_1=\ell_2=1$. Here, the far-field phase profiles show that both the 13th and 14th harmonic carry an OAM of $\ell_{H_{13}}=\ell_{H_{14}}=9$. According to the selection rules (1) for HHG

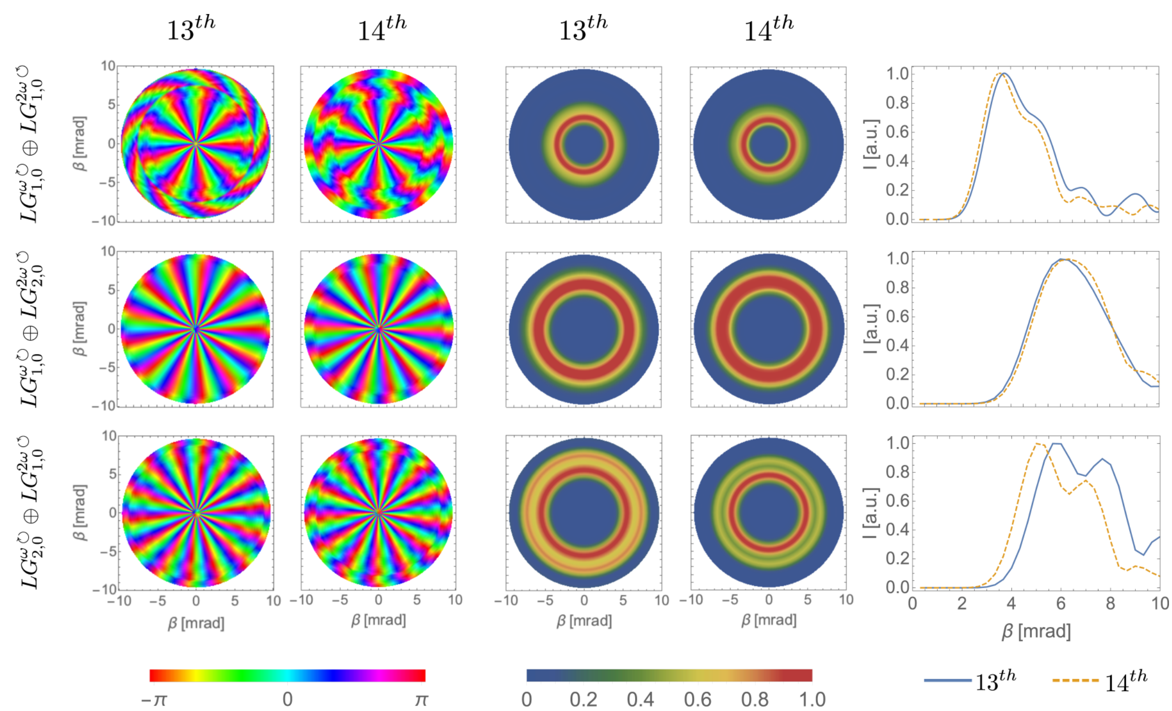

FIG. 2. Far-field phase (columns 1 and 2), intensity (columns 3 and 4) profiles, and a lineout through the intensity profiles (column 5) for 13th and 14th harmonic generated by a superposition of two counter-rotating LG modes $\mathrm{LG}_{\ell_1,0}^{\omega\circlearrowright} \oplus \mathrm{LG}_{\ell_2,0}^{2\omega\circlearrowleft}$ with different combinations of (ℓ_1,ℓ_2). Upper row $(\ell_1,\ell_2) = (1,1)$, middle row (1,2), lower row (2,1). For a better comparison of the intensity distributions, the maximum of each intensity profile was normalized to 1.

with bicircular fields, $m = 5$ photons of frequency ω and $n = 4$ photons of frequency 2ω contribute to the 13th harmonic. Since the OAM has to be conserved [26,27], the OAM of the 13th harmonic is given by $\ell_{H_{13}} = 5 \times 1 + 4 \times 1 = 9$. Similarly, in order to generate the 14th harmonic, $m = 4$ photons of frequency ω and $n = 5$ photons of frequency 2ω have to be absorbed. Hence, the 14th harmonic also carries an OAM of $\ell_{H_{14}} = 9$. Moreover, the 13th harmonic carries a SAM of 1 and the 14th a SAM of -1, respectively. The selection rules for HHG with bicircular LG beams can be summarized as Eq. (2).

The middle row of Fig. 2 shows the far-field phase profiles of the 13th and the 14th harmonic for a superposition of a $\mathrm{LG}_{1,0}^{\omega\circlearrowright}$ and a $\mathrm{LG}_{2,0}^{2\omega\circlearrowleft}$ beam. As a result, we find that the qth harmonic carries an OAM of q, which is confirmed by Eq. (2). In the lower row, we display the 13th and 14th harmonic from HHG by a superposition of a $\mathrm{LG}_{2,0}^{\omega\circlearrowright}$ beam and a $\mathrm{LG}_{1,0}^{2\omega\circlearrowleft}$ beam. Here, the 13th harmonic carries an OAM of 14 and the 14th harmonic an OAM of 13, respectively.

However, from an experimental point of view the question arises whether we can generate a specific harmonic with an arbitrary value of OAM and, if so, how to determine the OAM ℓ_1 and ℓ_2 of the incident beams. The first two equations in (2) are the same as the selection rules for HHG in bicircular fields. For the qth harmonic we can find m and n by the integer solutions of

$$m = \frac{q \pm 2}{3} \quad \text{and} \quad n = \frac{q \mp 1}{3}. \tag{5}$$

However, since every third harmonic is suppressed, we cannot obtain integer solutions for m and n, if q is dividable by three. Moreover, we still have to clarify whether we can get ℓ_1 and ℓ_2 for an arbitrary ℓ_{H_q} to fulfill $\ell_{H_q} = m\,\ell_1 + n\,\ell_2$. This equation is known as a linear Diophantine equation [28]. Since $m - n = \pm 1$, we can always find integer solutions for the Diophantine equation. In order to get all possible solutions for ℓ_1 and ℓ_2, we first solve the homogeneous equation $0 = m\,\ell_1 + n\,\ell_2$ and find one particular solution afterwards. The set of solutions can be expressed as a superposition of the homogeneous and particular solution. The solutions of the homogeneous equation can be written as

$$\ell_1 = a\,n \quad \text{and} \quad \ell_2 = -a\,m \quad \text{for } a \in \mathbb{Z}. \tag{6}$$

We have to find the particular solution for two cases, namely, $m - n = 1$ and $m - n = -1$. For the first mentioned, we obtain $(\ell_1, \ell_2) = (\ell_{H_q}, -\ell_{H_q})$, and for the latter one, we find $(\ell_1, \ell_2) = (-\ell_{H_q}, \ell_{H_q})$. Note that ℓ_{H_q} can be negative as well. In order to get the general solution of the Diophantine equation we now combine the homogeneous solution (6) with the corresponding particular solution, which is summarized in Table I.

Moreover, the analysis is not restricted to ω-2ω bicircular fields, but can be applied to arbitrary bicircular fields. Generically, we show the results for ω-3ω and $r\omega$-$s\omega$ bicircular fields in Table I. However, for ω-3ω bicircular fields, all even harmonics are suppressed due to the selection rules.

Besides the analysis of the phase profile of the emitted radiation, we also considered their divergence. In the middle part of Fig. 2 we display the far-field intensity profile for each harmonic from the left part of the same figure, while the right column shows a lineout of the intensity profiles for the 13th (blue, solid) and 14th (orange, dashed) harmonic. In the upper

TABLE I. Parameters of the incident bicircular LG beams for generating high-order harmonics with selected OAM ℓ_{H_q}. Apart from the frequency ratio of the counter-rotating beams (first column), we here show the harmonic order and the OAM of the emitted harmonic (second and third column). In the fourth and fifth columns we calculated m and n, respectively the number of photons from the first and second incident beams which are necessary to obtain the qth harmonic. The column labeled with SAM gives the SAM of the qth harmonic, where we assumed the first beam to carry a SAM of 1 and the second beam a SAM of -1, respectively. The last two columns can be used to determine the required OAM of the incident beams in order to generate the qth harmonic with an OAM of ℓ_{H_q}. Here, a is an arbitrary integer.

Frequencies	Harmonic order	OAM	m	n	SAM	ℓ_1	ℓ_2
$\omega+2\omega$	$q=m+2n$	ℓ_{H_q}	$\frac{q\pm 2}{3}$	$\frac{q\mp 1}{3}$	$m-n=1$	$\ell_{H_q}+a\,n$	$-\ell_{H_q}-a\,m$
	$q=1,2,4,5,\ldots$				$m-n=-1$	$-\ell_{H_q}+a\,n$	$\ell_{H_q}-a\,m$
$\omega+3\omega$	$q=m+3n$	ℓ_{H_q}	$\frac{q\pm 3}{4}$	$\frac{q\mp 1}{4}$	$m-n=1$	$\ell_{H_q}+a\,n$	$-\ell_{H_q}-a\,m$
	$q=1,3,5,7,\ldots$				$m-n=-1$	$-l_{H_q}+a\,n$	$l_{H_q}-a\,m$
$r\omega+s\omega$	$q=rm+sn$	ℓ_{H_q}	$\frac{q\pm s}{r+s}$	$\frac{q\mp r}{r+s}$	$m-n=1$	$\ell_{H_q}+a\,n$	$-\ell_{H_q}-a\,m$
	$q=r,s,2r+s,2s+r,3r+2s,3s+2r,\ldots$				$m-n=-1$	$-\ell_{H_q}+a\,n$	$\ell_{H_q}-a\,m$

row, we see that the radius of the annular intensity profile for the 13th (left intensity profile or blue, solid lineout) harmonic is slightly larger than for the 14th harmonic (right intensity profile or orange, dashed lineout). In the middle row, the shown harmonics carry the OAM of their harmonic order. Here, the far-field intensity profiles show a similar divergence, which reconfirms the findings for HHG with a single linearly polarized LG mode, where all harmonics are emitted with a similar divergence, if the OAM scales with the harmonic order [11]. In the lower row we display the far-field profile the 13th harmonic, which carries an OAM of $\ell_{H_{13}}=14$ and the 14th harmonic with an OAM $\ell_{H_{14}}=13$. In particular, the OAM decreased with the harmonic order. It can be seen that the divergence of the 13th harmonic is higher than the divergence of the 14th harmonic.

In order to derive a quantitative expression for the divergence in the far-field intensity distribution from the Frauenhofer diffraction formula (4), we express the complex amplitude in the near field ($z=0$) for the qth harmonic as

$$A_q^{\mathrm{near}}(\rho',\phi')=f(\rho')\exp[i(\ell_{H_q})\phi'], \tag{7}$$

where $f(\rho')$ is a function that contains all radial quantities [29] and $\ell_{H_q}=m\ell_1+n\ell_2$ is the OAM of the qth harmonic [cf. Eq. (2)]. The integral over ϕ' in Eq. (4) can be performed analytically [30] and takes the form of a Hankel transform. As a result, we express the far-field amplitude as [11]

$$A_q^{\mathrm{far}}(\beta,\phi)=-\frac{1}{2\pi i^{\ell_{H_q}}}\exp\left(i\ell_{H_q}\phi\right)\times\int_0^\infty d\rho'\,\rho' f(\rho')J_{\ell_{H_q}}\left(\frac{2\pi}{\lambda_q}\beta\rho'\right). \tag{8}$$

The integrand scales with a Bessel function of the order of the OAM ℓ_{H_q} of the emitted radiation. However, the argument of the Bessel function is inversely proportional to the wavelength of the qth harmonic, or, more specifically, proportional to the harmonic order. The value of β, where the Bessel function reaches its maximum, can be interpreted as the divergence. While the divergence of the emitted radiation increases as the OAM ℓ_{H_q} increases, the divergence of the harmonic decreases as the harmonic order increases. Especially, the divergence of the harmonics is found to be similar if the OAM increases with the harmonic order [11,29].

The intensity profiles in the bottom row show an additional distinct concentric ring. The occurrence of additional rings was already observed in HHG with linearly polarized LG beams and attributed to the interplay of short and long trajectories [22,31]. The lineouts in the right column show that there are additional rings for a superposition of $\mathrm{LG}_{1,0}^{\omega\circlearrowright}\oplus\mathrm{LG}_{1,0}^{2\omega\circlearrowleft}$ as well, although they are much weaker than those for a $\mathrm{LG}_{2,0}^{\omega\circlearrowright}\oplus\mathrm{LG}_{1,0}^{2\omega\circlearrowleft}$. Our simulations showed that the additional rings are more distinct, if the $\mathrm{LG}^{2\omega\circlearrowleft}$ beam dominates the radial intensity distribution across the focus after the intensity maximum. Nevertheless, a detailed analysis of the contributions of the short and long trajectories to the harmonic spectrum has to be performed, in order to fully understand the occurrence of the additional rings.

In conclusion, we showed that HHG with two-color counter-rotating LG modes can be used to obtain circularly polarized XUV vortices. Moreover, we extended the selection rules from HHG with bicircular fields to include also the conservation of OAM. Especially, the OAM of the emitted radiation can by controlled by the incident LG modes. We showed that an arbitrary value of the OAM can be imprinted on a harmonic by a proper choice of the incident LG modes. In addition, we explained how to calculate the OAM of the incident beams to observe a selected harmonic with a specific OAM. Finally, we discussed the divergence of the emitted harmonics with respect to their order and their OAM and reconfirmed the findings from HHG with linearly polarized LG modes. Despite the circular polarization of each harmonic, the resulting attosecond pulse trains are linearly polarized. Thus it would be interesting to see if it is possible to suppress the left or right circularly polarized harmonics in order to achieve circularly polarized XUV attosecond pulse trains with OAM, similar to Ref. [17].

This work was financially supported within the priority programme QuTiF from German Science Foundation (DFG) under Contract No. FR 1251/17-1.

[1] L. Allen, M. W. Beijersbergen, R. J. C. Spreeuw, and J. P. Woerdman, Phys. Rev. A **45**, 8185 (1992).
[2] M. Padgett, J. Courtial, and L. Allen, Phys. Today **57**(5), 35 (2004).
[3] R. A. Müller, D. Seipt, R. Beerwerth, M. Ornigotti, A. Szameit, S. Fritzsche, and A. Surzhykov, Phys. Rev. A **94**, 041402 (2016).
[4] A. A. Peshkov, V. G. Serbo, S. Fritzsche, and A. Surzhykov, Phys. Scr. **91**, 064001 (2016).
[5] A. Surzhykov, D. Seipt, and S. Fritzsche, Phys. Rev. A **94**, 033420 (2016).
[6] T. Kuga, Y. Torii, N. Shiokawa, T. Hirano, Y. Shimizu, and H. Sasada, Phys. Rev. Lett. **78**, 4713 (1997).
[7] M. P. J. Lavery, F. C. Speirits, S. M. Barnett, and M. J. Padgett, Science **341**, 537 (2013).
[8] M. Zürch, C. Kern, P. Hansinger, A. Dreischuh, and C. Spielmann, Nat. Phys. **8**, 743 (2012).
[9] C. Hernández-García, A. Picón, J. San Román, and L. Plaja, Phys. Rev. Lett. **111**, 083602 (2013).
[10] G. Gariepy, J. Leach, K. T. Kim, T. J. Hammond, E. Frumker, R. W. Boyd, and P. B. Corkum, Phys. Rev. Lett. **113**, 153901 (2014).
[11] R. Géneaux, A. Camper, T. Auguste, O. Gobert, J. Caillat, R. Taïeb, and T. Ruchon, Nat. Commun. **7**, 12583 (2016).
[12] P. B. Corkum, Phys. Rev. Lett. **71**, 1994 (1993).
[13] P. Agostini and L. F. DiMauro, Rep. Prog. Phys. **67**, 813 (2004).
[14] P. Salières and M. Lewenstein, Meas. Sci. Technol. **12**, 1818 (2001).
[15] D. B. Milošević, W. Becker, and R. Kopold, Phys. Rev. A **61**, 063403 (2000).
[16] E. Pisanty and A. Jiménez-Galán, Phys. Rev. A **96**, 063401 (2017).
[17] A. Jiménez-Galán, N. Zhavoronkov, D. Ayuso, F. Morales, S. Patchkovskii, M. Schloz, E. Pisanty, O. Smirnova, and M. Ivanov, Phys. Rev. A **97**, 023409 (2018).
[18] K. M. Dorney, J. L. Ellis, C. Hernández-García, D. D. Hickstein, C. A. Mancuso, N. Brooks, T. Fan, G. Fan, D. Zusin, C. Gentry, P. Grychtol, H. C. Kapteyn, and M. M. Murnane, Phys. Rev. Lett. **119**, 063201 (2017).
[19] A. Fleischer, O. Kfir, T. Diskin, P. Sidorenko, and O. Cohen, Nat. Photon. **8**, 543 (2014).
[20] D. B. Milošević, J. Phys. B **48**, 171001 (2015).
[21] E. Pisanty, S. Sukiasyan, and M. Ivanov, Phys. Rev. A **90**, 043829 (2014).
[22] L. Rego, J. S. Román, A. Picón, L. Plaja, and C. Hernández-García, Phys. Rev. Lett. **117**, 163202 (2016).
[23] M. Lewenstein, P. Balcou, M. Y. Ivanov, A. L'Huillier, and P. B. Corkum, Phys. Rev. A **49**, 2117 (1994).
[24] E. Pisanty, RB-SFA: High Harmonic Generation in the Strong Field Approximation via Mathematica, https://github.com/episanty/RB-SFA, v2.1.2 (2016).
[25] M. Born and E. Wolf, *Principles of Optics: Electromagnetic Theory of Propagation, Interference and Diffraction of Light* (Cambridge University Press, Cambridge U.K., 1999).
[26] F. Kong, C. Zhang, F. Bouchard, Z. Li, G. G. Brown, D. H. Ko, T. J. Hammond, L. Arissian, R. W. Boyd, E. Karimi, and P. B. Corkum, Nat. Commun. **8**, 14970 (2017).
[27] D. Gauthier, P. R. Ribič, G. Adhikary, A. Camper, C. Chappuis, R. Cucini, L. F. DiMauro, G. Dovillaire, F. Frassetto, R. Géneaux, P. Miotti, L. Poletto, B. Ressel, C. Spezzani, M. Stupar, T. Ruchon, and G. D. Ninno, Nat. Commun. **8**, 14971 (2017).
[28] M. Hazewinkel, *Encyclopaedia of Mathematics (set)* (Springer, Berlin, 1994).
[29] C. Hernández-García, J. S. Román, L. Plaja, and A. Picón, New J. Phys. **17**, 093029 (2015).
[30] N. M. Temme, *Special Functions: An Introduction to the Classical Functions of Mathematical Physics* (Wiley-Interscience, New York, 1996).
[31] R. Géneaux, C. Chappuis, T. Auguste, S. Beaulieu, T. T. Gorman, F. Lepetit, L. F. DiMauro, and T. Ruchon, Phys. Rev. A **95**, 051801 (2017).